29B TECHNICAL REPORT-70; END

MAGNETIC AND VELOCITY EFFECTS ON IONOSPHERIC ELECTRON CURRENT TO CYLINDRICAL ELECTROSTATIC PROBES

BY

NATHAN J. MILLER

UNIVERSITY OF MARYLAND
DEPARTMENT OF PHYSICS AND ASTRONOMY
COLLEGE PARK, MARYLAND

AUGUST 1967

APPROVAL SHEET

Title of Thesis: Magnetic and Velocity Effects on Ionospheric Electron Current to Cylindrical Electrostatic Probes

Name of Candidate: Nathan J. Miller
Master of Science, 1967

Thesis and Abstract Approved:

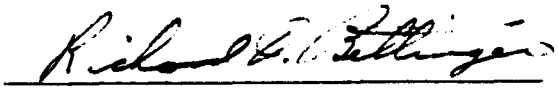

Richard T. Bettinger
Assistant Professor of Physics
Department of Physics and Astronomy

Date Approved: 7/26/67

VITA

Name: Nathan John Miller

Permanent Address: #701, 1101 Third Street, S. W.
Washington, D. C. 20024

Degree and date to be conferred: Master of Science, 1967

Date of Birth: [redacted]

Place of Birth: [redacted]

Secondary Education: Bartlett High School, 1953

Collegiate Institutions Attended:	Dates	Degree	Date of Degree
Nebraska University, Lincoln, Nebraska	1953-1960	B. S.	1958
University of Maryland, College Park, Md.	1961-1967	M. S.	1967

Major: Physics

Positions Held: Graduate Teaching Assistant, Physics Department, Nebraska University, 1958-1960.

Physicist, National Bureau of Standards, Washington, D. C., 1960-1962.

Aerospace Technologist, Goddard Space Flight Center, Greenbelt, Maryland, 1962-1967.

ABSTRACT

Title of Thesis: Magnetic and Velocity Effects on Ionospheric Electron Current to Cylindrical Electrostatic Probes.

Nathan J. Miller, Master of Science, 1967

Thesis directed by: R. T. Bettinger, Assistant Professor of Physics

Ionospheric measurements made with cylindrical electrostatic probes show fluctuations in the current collection due to both the satellite velocity and the earth's magnetic field. These fluctuations represent deviations from the Mott-Smith and Langmuir theory for current collection by electrostatic probes. The present analysis of electron current data from the Explorer 31 satellite probe experiment shows the satellite velocity effects and the magnetic field effects to be resolvable into separate velocity and magnetic field modulations of current which are superimposed upon some constant electron current. After separation, the manner in which each effect arises is explored in a manner consistent with the data.

The results indicate that ionospheric electron current measurements in the accelerating region for cylindrical electrostatic probes may contain a velocity modulation which could increase the current by a factor of two or reduce it by one-half. If the velocity modulations are accounted for, the magnetic modulations can cause fluctuations of from 20 - 60% in the remaining current. Since such current measurements are used to deduce ionospheric electron densities, these velocity and magnetically related electron current modulations should be considered in evaluating ionospheric electrostatic probe data.

MAGNETIC AND VELOCITY EFFECTS ON IONOSPHERIC ELECTRON CURRENT TO CYLINDRICAL ELECTROSTATIC PROBES

by

Nathan J. Miller

August 1967

Thesis submitted to the Faculty of the
Graduate School of the University
of Maryland in partial fulfillment of
the requirements for the degree of
Master of Science
1967

ACKNOWLEDGEMENTS

To all who have aided in the creation of this thesis, I express my thanks. In particular, I thank my advisor, Dr. R. T. Bettinger, who suggested the problem, for providing guidance and moral support; Larry Brace for allowing me to pursue this study; John Saylor for supplying me with data; and Mrs. Donna Will for patiently typing the manuscript. This work has been supported in part by The National Aeronautics and Space Administration Grant NGR-21-002-060.

TABLE OF CONTENTS

FIGURE CAPTIONS

Figure 1 Illustration of the ionospheric layer structure and the relation of electron density to total particle density.

Figure 2 Schematic view of the Explorer 31 satellite illustrating the relationship between the satellite probes, the geomagnetic field lines, and the satellite velocity. The angles indicated are measured satellite parameters.

Figure 3 Cylindrical probe characteristic illustrating the regions of differing current behavior. The reference voltage is arbitrarily taken at a region boundary.

Figure 4 Probe characteristic maxima plotted as a function of aspect angle for a seven minute time period of a northbound pass. Each curve is labeled by the geomagetic latitude at which the data was taken. The minimum aspect angle is 15^{o} and only forward aspect angles are considered.

Figure 5 Probe characteristic maxima plotted as a function of field angle for a seven minute time period of a northbound pass. Each curve is labeled by the geomagnetic latitude at which the data was taken.

Figure 6 Curves showing the variation of $I(\theta,\phi)$ at 750 km with aspect angle where the numbers beside each data point are the values of ϕ in degrees. The curves are labeled by the pass numbers from which the data came.

CHAPTER I

THE IONIZED COMPONENT OF THE EARTH'S ATMOSPHERE

Introduction

In terms of significant ionization, the earth's ionized atmosphere extends from near 50 km to the boundary of the earth's magnetic field. However, charged particles are a minor constituent of the earth's atmosphere until altitudes near 1500 km where neutral and charged particle densities become comparable. The charged particle density increases to an altitude near 400 km. Above that height, the decreasing atmospheric density causes the ion density to decrease with altitude, though the percentage of ionization continues to increase.

The Ionosphere

The term "ionosphere" could be applied to the total altitude range of atmospheric ionization, but the ionosphere proper is that portion of the earth's atmosphere which significantly influences ground-based radio wave propogation. This definition is used because it was through radio wave interactions that the charged particle region between 60 and 400 km was discovered. Radio wave reflection occurs whenever the free electron density of a medium changes. However, total reflection occurs whenever the radio frequency is less than a critical frequency ω_p, termed the plasma frequency which is specified by the electron density n_e through the relation

$$\omega_p = \left(\frac{n_e e^2}{m\varepsilon}\right)^{\frac{1}{2}}$$

The properties of the medium containing the free electrons is accounted for by the term ε, the permitivity of the medium while m and e are the electronic mass and charge respectively. Since n_e is the free electron number denisty at a point in space, scanning a frequency range of radiowaves sent upward from the earth and noting the time interval between emission and reception leads to an altitude profile of electron density, so long as the density is increasing. Ground-based studies have implied a layered structure for the ionosphere, as shown in Figure 1. Each ionization layer is specified by a letter.

The lower D region is sometimes referred to as the C region and extends between 50 and 70 km. The C region has associated with it a maximum electron density near 10^2/cc. The ionization source is cosmic ray interactions with the neutral atmosphere. The electron density disappears at night and maintains its maximum value at a constant height during daytime. This behavior results from an attachment of electrons to neutrals. The resulting negative ion is readily dissociated by sunlight.

$$O_2 + e + M \rightarrow O_2^- + M$$

Electron Attachment

$$O_2^- + h_\nu \rightarrow O_2 + e$$

Photodetachment

Cosmic rays penetrate below the C region but attachment processes are

strong enough and solar radiation transmission is weak enough to make the free electron density negligible.

The most important process for producing D region ionization is the photoionization of NO by Lyman - α solar radiation (Nicolet and Aiken, 1960).

$$NO + h\nu \rightarrow NO^+ + e$$

This region forms between 70 and 85 km and has associated with it a maximum of electron density near 10^3/cc. The altitude maximum electron density increases with decreasing solar zenith angle in a predictable manner during the daytime. The nighttime electron density effects on radio waves become negligible because of electron losses in dissociative recombination reactions and electron attachment to neutrals.

$$\{N_2^+,\ O_2^+\} + e \rightarrow \begin{cases} N + N \\ O + O \end{cases}$$

Dissociative Recombination

Atmospheric NO is only present in small quantities but it appears that the amount present is sufficient to account for NO as the principle ion in the D region. Some ions must be formed from x-ray photoionization of O_2 and N_2 because there is a solar cycle effect in the electron density variations which does not occur in the Lyman - α radiation.

The altitude range between 85 and 150 km is the E region, which has a daytime electron density maximum near 10^4/cc. This region

forms a transition from a realm in which charged particle motions are constrained by the geomagnetic field. In the E region, the electron motions are governed by the magnetic field lines and the ion motions are governed by the neutral particle motions. This behavior pattern emerges because the electron-neutral collision frequencies have decreased sufficiently for magnetic effects to be important while the ion motions are still collision dominated. The neutral particle motions also are changing in the E region, from a condition of convective equilibrium which existed below, to a condition of diffusive equilibrium. The result is that the altitudinal distribution of neutral particles is approximately described by the barometric formula

$$\frac{d \ln n_s}{dZ} = \frac{m_s g}{k T_s}$$

which applies for diffusive equilibrium conditions. Z represents the altitude, n_s is the number density of one neutral constituent, m_s and T_s are the mass and temperature of the same constituent, g is the gravitational acceleration at height Z, and k is the Boltzmann constant. The ionization is formed by photoionization of O, O_2, and N_2 by normal solar x-ray flux. As with the D region, the height of the daytime electron density maximum increases in a predictable manner with decreases in solar zenith angle. However, radio wave effects continue at night because of ionization from meteors, and decreased recombination and electron attachment reactions.

In the F region, which lies between 150 and 400 km, the neutral

particles have reached diffusive equilibrium. The principle ionization reaction is solar ultraviolet photoionization of O. The continuing decrease in atmospheric density with increasing altitude has a great impact upon the charged particles in this region. The collision frequencies have decreased enough that both ion and electron motions are constained by the magnetic field lines; transport into and out of the upper F region is great enough that the ion composition can no longer be predicted by local chemical processes alone; lastly, the electron loss mechanism charges from one in which dissociative recombination determines the loss rate to one in which the ion-atom interchange reactions are rate determining.

$$\left.\begin{matrix} N_2^+ + O \\ N_2 + O^+ \end{matrix}\right\} \rightarrow NO^+ + N \qquad\qquad NO^+ + e \rightarrow N + O$$

Ion-Atom Interchange Followed By Dissociative Recombination

The last effect leads to two maxima of electron density, the F_1 maximum with electron densities near 10^5/cc around 200 km, and the F_2 maximum between 300 and 400 km with electron densities near 10^6/cc. The F_1 maximum occurs in the vicinity of the F region photoionization maximum. Near this same position, the loss mechanism changes form. The photoionization above the F_1 peak depends on the concentration of O whereas the loss rate by ion-atom interchange depends on the concentration of N_2. Since the N_2 density decreases with altitude much more rapidly than the O density, the loss rate for electrons decrases much more rapidly than the production rate resulting in an increasing electron density as the altitude increases to the position of the F_2 maximum. The

height of the F_1 maximum increases with decreasing solar zenith angle until it merges with the F_2 maximum. The F_2 maximum is present during both day and night. Its behavior is not well correlated with that of normal solar radiation, hence the current view is that there is an important secondary ionization source for the F_2 region, (Antonova and Ivanov-Kholodnyy, 1961).

The Topside Ionosphere

The topside ionosphere is the ionized atmosphere above the F_2 maximum. The bottomside ionosphere can be characterized as a region in which photo-chemical processes strongly influence the charged particle composition. The equation describing chemical equilibrium is of the form

$$\frac{dn(XY^+)}{dt} = q - L = 0$$

where

$$n(XY^+)$$

is the density of a molecular ion XY^+. q is the production rate for XY^+ and generally is of the form $k_\lambda F_\lambda n(XY)$ where k_λ is a production rate coefficient and F_λ is the solar flux for a given wavelength interval. L is the loss rate and generally is of the form $\alpha n_e n(XY^+)$ where α is a recombination coefficient for dissociative recombination and n_e is the ambient electron density. At the F_2 maximum, chemical processes and transport processes have become equal in importance, so the continuity equation for an ionic species must add a transport term and take the form

$$\frac{dn(XY^+)}{dt} = q - L - \frac{d\, n(XY^+)v}{ds}$$

where v is the ionic transport velocity and s is distance along a magnetic field line. Within the topside ionosphere, transport processes become the dominant factor in determining the charged particle composition. Therefore, the topside ionosphere can be characterized as the region of the ionosphere in which the charged particles approach diffusive equilibrium.

At topside altitudes, the neutral particle collision frequencies are so small that the neutrals perform ballistic motions. If neutral particles velocities are high enough particles can escape from this neutral exosphere. Standard gas laws based on fluid behavior no longer describe the neutral density distribution (Chamberlain, 1963) under these circumstances. In contrast, the long range coulomb forces guarantee that charged particle collision frequencies will remain important in the topside ionosphere.

Because of coulomb interactions, the diffusive equilibrium which charged particles can attain is a modified form of the diffusive equilibrium which neutrals reach. For a single ionic species, diffusive equilibrium is described by the equation

$$\frac{d \ln n_s}{dz} = -\frac{m_s g}{k(T_e + T_i)}$$

where T_i and T_e are the temperatures of the ions and electrons respectively. The equation is similar to the barometric equation for neutrals except that the ion and electron temperatures must be

considered separately. The difference in form occurs because there can be no appreciable charge separation between ions and electrons. The electrons, which from mass considerations should diffusive to much greater heights than any ion, must drag the ions along because charge separation produces polar electric fields which act on the ions. The result is that ions diffuse to much greater heights than would neutrals of the same mass and temperature. In the topside ionosphere, the charged particles must diffuse along magnetic field lines and also there is more than one ionic species present at a time. Both factors modify the manner in which diffusion takes place among charged particles and can produce situations in which diffusive equilibrium requires that the density of a minor ion should increase with altitude.

The principal ions in the topside ionosphere are O^+, H^+, and He^+. The process for ion production is photoionization of the atoms by normal solar x-rays and ultraviolet radiation. Coupling between the topside ionosphere above 1000 km and the F region of the ionosphere has been investigated in an attempt to explain the nighttime F_2 peak (Geisler and Bowhill, 1965). It was found that magnetically aligned charged particle fluxes between the topside ionosphere and the F region of the ionosphere would be insufficient to account for the nighttime F_2 maximum. However, it was found that fluxes of photoelectrons flowing from the F region to the daytime topside ionosphere could explain the topside electron temperature structure. At night then, there would be charged particle fluxes from the topside ionosphere to the F region. The character of the ion transport changes at various altitudes causing

the degree to which diffusive equilibrium is approached to vary similarly. For example, near the F_2 maximum the diffusion is O^+ through a predominately atomic oxygen atmosphere; near 700 km the diffusion is H^+ through a mixture of O and He. The data presented in this thesis was taken in the region above 700 km where H^+ is the major diffusing ion.

CHAPTER II

THE EXPLORER 31 ELECTROSTATIC PROBE EXPERIMENT

Introduction

The Explorer 31 satellite was launched on November 29, 1965 into an elliptical orbit about the earth. The orbit apogee is 3000 km and the perigee is 500 km. The satellite's spin axis is nearly perpendicular to the satellite translational velocity. The satellite carries a number of experiments to measure atmospheric parameters, among which is a Langmuir probe experiment. This consists of two cylindrical electrostatic probes mounted near the bottom of the satellite and at opposite ends of a satellite diameter.

The cylindrical electrostatic probes are conducting wires which extend into the ionized medium and are connected to a voltage generator on the satellite. The schematic diagram in Figure 2 shows the relationship between the probes and the satellite's translational velocity while the satellite rotates. The experimental procedure is to monitor the current drawn as the probe voltage is swept in 1 second from -2 to +5 volts relative to the satellite potential. At the endpoint of a voltage sweep, satellite spatial relationships are measured, e. g. the angle between the probe axis and the sun direction. While one probe is being used for measurements appropriate to electron temperature determinations, the other is being used for measurements appropriate to the determination of electron densities. The wake region of the satellite path is not suitable for making these measurements and,

therefore, meaningful temperature and density determinations are separated in time by at least the time necessary for the satellite to rotate through 180°. This time is 10 seconds and represents a spatial distance of 80 km.

Measurement Theory

The theory of electrostatic probe current collection was summarized by Mott-Smith and Langmuir in 1926. When a conductor is immersed into the ionospheric plasma, it will normally become negatively charged because the electrons move faster than the ions and, therefore, accumulate faster. The limit of the charge buildup is reached when incoming electrons and ions are affected by the negative charge to the extent that the flux of ions and electrons to the conductor becomes equal, resulting in no net current. The potential distribution about the negatively charged conductor is only significant over a limited region of space surrounding the conductor known as the plasma sheath. Essentially all of the potential difference between the conductor and the plasma falls within this sheath. Therefore, the theory assumes that all plasma particles beyond the sheath behave as though the conductor were not present.

The thermal motions of charged particles cause some to diffuse into a sheath region where they are affected by the potential distribution. If the potential on a conductor is varied, as is done with an electrostatic probe, the sheath dimensions will vary similarly. However, under the assumptions of no collisions within the sheath region (Mott-Smith and Langmuir, 1926), it was found that the current to an

infinite cylindrical probe was independent of the sheath dimensions and potential distribution so long as the sheath radius was much larger than the probe radius and the potential distribution was monotonic. The probe equations correlate with observed cylindrical probe characteristics as typified by the one in Figure 3.

The equation

$$j = \frac{ne\bar{v}}{4}\left(\frac{2}{\sqrt{\pi}}\right)\left(1 + \frac{eV}{kT}\right)^{\frac{1}{2}}$$

where j is current density, describes the ion or electron flux to a cylindrical probe at rest in the ion or electron accelerating region of a cylindrical probe characteristic curve for a Maxwellian velocity distribution whenever $eV \geq 5kT$.

n = the number density of the charged species

e = the electronic charge

T = the temperature of the charged species

k = the Boltzmann constant

$\bar{v} = \left(\frac{8kT}{\pi M}\right)^{\frac{1}{2}}$ = the mean velocity of a Maxwellian velocity distribution

V = the probe potential relative to the plasma potential

The electron accelerating region is the voltage range where the probe is positive enough to repulse all ions resulting in only electron current collection. The ion accelerating voltage range is a negative counterpart to the electron accelerating range. The accelerated charged particle current can be used to deduce charged particle densities from the current equation.

In the electron retarding voltage region the probe has a

negative potential but some of the electrons are energetic enough to reach the probe anyhow. The electrons arriving at the probe cancel some of the ion flux which the negative probe attracts. The equation

$$j = \frac{ne\bar{v}}{4} \exp[eV/kT]$$

applies to the retarded electron component of the charged particle flux to the probe in this region. The retarded electron current can be used to determine electron temperatures from the current equation.

Measurement Results

Satellite measurements in the ionosphere introduce complications into electrostatic probe theory since the satellite velocity and the magnetic field both affect the charged particle flux to the probe. We define the angle between the probe axis and the velocity of the satellite to be the aspect angle, θ, and the angle between the probe axis and the magnetic field direction to be the field angle, ϕ. Determinations of both of these angles are made at the ends of the probe voltage sweeps and their values appear on data sheets along with the probe current values. Plots of the raw current values at the positive maxima of the probe characteristics taken from the Explorer 31 satellite data yield results similar to the plots in Figures 4 and 5. The data was taken while the satellite was traversing its orbit through changing altitudes and electron densities. Since this data only includes current taken as a satellite probe rotated into the forward direction of the satellite's orbital motion, what would appear as a single curve, increasing or decreasing monotonically in time, appears on the graphs

as unconnected curves because of the omission of wake region data. Moreover, there is the presence of a periodic fluctuation within the data producing minima and maxima at various aspect angles. The plots of data show that the periodic fluctuations are related to both the aspect and field angles, hence, it is desirable to separate the current modulation into its components before attempting to explain the variations which appear.

The first assumption in the separation procedure is that in the electron accelerating region of the cylindrical probe characteristics, the electron current divided by the square root of the probe potential relative to the plasma potential is proportional to the electron density. Taking note of the equation describing the probe electron current for this voltage region shows that this is equivalent to assuming that eV/kT is enough greater than 1 to ignore the 1 in $(1 + eV/kT)^{\frac{1}{2}}$. For the data that was analyzed $eV/kT \geq 5$ which makes a maximum error of 9% resulting from this assumption.

The time for a probe to rotate through the forward aspect angles on the Explorer 31 satellite is 10 seconds during which there should be only slight variations in the electron density. Therefore, a plot of $I/V^{\frac{1}{2}}$ values taken at the maxima of the probe characteristics against forward aspect angle should give a series of nearly straight horizontal lines. The fact that this is not the case is due to the modulations caused by satellite velocity and magnetic field effects in the ionosphere, which leads to the next assumption in the separation procedure. The reference level for velocity induced modulations is arbitrarily defined

as zero at 90^{o} aspect angle. Under these conditions, the electron current to a rotating cylindrical probe with an orbital motion in the ionosphere would draw the same current at 90^{o} aspect angle as the same probe without its orbital motion, i.e. there is only a magnetic field modulation of current.

Another assumption in separating magnetic and velocity effects on ionospheric probe current is that the velocity modulation of current should be strictly symmetrical about $\theta = 0$, and a function which gives the magnetic modulation of current should be nearly symmetrical about $\phi = 90^{o}$. The objective of the separation is to obtain the two functions, $V(\theta)$ and $M(\phi)$. $V(\theta)$ gives the satellite velocity induced modulation of $I/V^{\frac{1}{2}}$ as a function of field angle.

Define the experimental values of $I/V^{\frac{1}{2}}$ as the function $I(\theta,\phi)$. Then $I(\theta,\phi) = V(\theta) + M(\phi)$ where $V(\phi)$ and $M(\phi)$ have been defined and any interaction between velocity and magnetic effects has been assumed to be constant or negligible. $V(\theta)$ is zero at $\phi = 90^{o}$ and is symmetrical about $\theta = 0^{o}$. $M(\phi)$ represents the unperturbed electron current with a magnetically modulated current added. The first step in the separation procedure is to make one plot of $I(\theta,\phi)$ against forward aspect angle and another plot of $I(\theta,\phi)$ against field angle, where the data is taken at the maxima of the probe characteristics. For each value of $I(\theta,\phi)$, there corresponds a field angle and an aspect angle which are coupled to each other. $I(\pm 90^{o},\phi_1) = M(\phi_1)$ because $V(\pm 90^{o}) = 0$. In the first approximation $M_1(\phi_1) = M_1(\phi_1')$ where ϕ_1 and ϕ_1' are supplements; therefore, $V_o(\theta_2) = I(\theta_2,\phi_1') - M_1(\phi_1') = I(\theta_2,\phi_1') - I(90^{o},\phi_1)$. Now $V_o(\theta_2) = V_o(-\theta_2)$, therefore,

$M_1(\phi_3) = I(-\theta_2,\phi_3) - V_o(-\theta_2)$. Since $M_1(\phi_3) = M_1(\phi_3')$, then, $V_o(\theta_4) = I(\theta_4,\phi_3') - M_1(\phi_3')$. $V_o(\theta_4) = V_o(-\theta_4)$ gives $M_1(\phi_5) = I(-\theta_4,\phi_5) - V_o(-\theta_4)$. Continuing in this vein allows one to get a first approximation, $M_1(\phi)$ to the function $M(\phi)$ by plotting the values $M_1(\phi_1)$, $M_1(\phi_1')$, $M_1(\phi_3)$, $M_1(\phi_3')$, etc. against ϕ. A numerical example of the first steps of the procedure is presented in the Appendix. The values of $M_1(\phi)$ can be compared with $I(\theta,\phi)$ to obtain the first approximation to $V(\theta)$.

If $V_1(\theta)$ is not symmetrical about zero aspect angle one can get a second approximation to $V(\theta)$ and $M(\phi)$ by drawing a mean curve for $V_1(\phi)$ which is the symmetrical $V_2(\phi)$. Then $I(\phi,\theta) - V_2(\theta) = M_2(\phi)$.

The results of applying this procedure to the data which appears in Figures 6 and 7 are shown in Figures 8 and 9. Similar results for data taken at other altitudes are shown in Figures 10 through 13. The final $V(\theta)$ curve represents the effect of a translational motion on the electron flux to a rotating satellite's electrostatic probe in the absence of a magnetic field where $V(\pm 90^o) = 0$. The final $M(\phi)$ curve represents the effect on the electron flux to a rotating satellite's electrostatic probe due to a magnetic field when there is no satellite orbital motion. The $M(\phi)$ curve shows the magnetic effect superimposed upon a constant current.

CHAPTER III

CONCLUSIONS

The results of probe measurements which have been presented illustrate the extent to which magnetic fields and satellite motion can affect electron current collected by cylindrical electrostatic probes. A mechanism for explaining these effects can be developed, by viewing the sheath surrounding a positively charged cylindrical probe as possessing a nearly uniform electron density, approximating that of the surrounding medium and a nonuniform ion density distribution. Within the sheath, the ion density will approach that of the surrounding medium with increasing radial distance from the probe. The sheath edge occurs at that surface where the sheath volume contains sufficient charge to "shield" the charge associated with the potential of the probe. Magnetic and velocity effects modify the sheath structure by changing the charged particle distribution within the sheath.

In general, discussions of the effects of satellite velocities upon electrostatic probe currents have not emphasized the case of electron currents in the accelerating region of probe characteristics because the thermal velocities for electrons are so much greater than the satellite velocities. However, the sheath structure for a positive probe is modified as a consequence of the satellite velocity. The results of the present data analysis suggest that current collection depends upon sheath structure. When the satellite traverses its orbit the satellite probe is rotating through a sea of electrons whose density

distribution is not greatly affected by the probe motion. However, the ion distribution in the probe sheath is affected because the ions do not move as rapidly as the probe. At 90° aspect angle, the ion distribution in the forward portion of the sheath is denser than in the rearward portion, resulting in a sheath which is not symmetrical about the probe axis. The spatial effect is that the sheath becomes elliptically shaped as shown in Figure 14. The equipotential surfaces which enclose circular areas near the probe, enclose elliptical areas as the sheath edge is approached. This deformation of sheath structure results in a modification in current collection as the aspect angle changes from 0° to 90°.

The Mott-Smith and Langmuir equations were derived for a sheath which was symmetrical about an infinite stationary cylindrical probe. These conditions are most nearly met at 0° aspect angle. However, the finite length of the probe makes current through the end of the cylindrical sheath a possibility. When the aspect angle is zero, the ion distribution near the end of the probe is altered because the ions are being overtaken by the probe. This situation requires that the sheath should extend farther from the probe end. The sheath deformation near the end of the probe causes extra amounts of electron current to be collected.

The velocity modulations of electron current depend upon the ion temperatures and masses rather than upon the electron properties as it is the ion motions which are producing the changes in sheath structures. The velocity modulation, neglecting end effects, decreases as ion temperatures increase because the ions are able to distribute themselves

about the probe more symmetrically at higher temperatures. In contrast, it has been suggested (Bettinger, 1966) that the end effect modulation for ion current to a negative cylindrical probe should increase in angular width as ion temperatures increase. Under the present mechanism one expects the same type of dependence for electron current to a positive probe. Combining these temperature effects suggests that at the lowest ion temperatures the function $V(\theta)$ should become increasingly negative at decreasing θ. As the ion temperatures increase, a positive effect will appear at small aspect angles which gradually increases in magnitude while the negative effects at larger aspect angles are gradually decreasing in magnitude. In some cases a temperature will be reached at which the negative and positive modulations cancel each other. Then $V(\theta) = 0$ for all $\theta \leq 90^{o}$. At the highest ion temperatures, only an end effect velocity modulation will appear, resulting in a positive valued $V(\theta)$ which increases in value as θ decreases. Examples of all of these conditions can be seen in the $V(\theta)$ curves presented in Figures 8, 10, and 12.

The magnetic field effects are complex to discuss because the charged particles are constrained to spiral about the magnetic field lines. This constraint means that the mean free path across the field lines is the gyro-radius of the particles and that charged particles move at faster rates along the field lines than across them. The concept of a guiding center, the position of the instantaneous center of the charged particle orbit, can be used to describe the charged particle motions along magentic field lines. The electrons which enter the probe sheath must have guiding centers that came from within a tube in space

of height (R_e + L sin ϕ + $2R_s$ cos ϕ) where L is the length of the probe including the sheath thickness at the end, R_e is the electron gyro-radius, R_s is the outer radius of the sheath, and ϕ is the field angle, excluding zero. The width of the tube is $2(R_s + R_e)$ when the field angle is zero. The satellite adds to the modulation effects since the satellite presence interferes with some of the flux which would normally enter the probe sheath and is the reason that the field tube cross section abruptly changes at zero field angle. Figure 15 illustrates the interception of the magnetic field lines by the satellite.

Because of the magnetic field constraints on charged particle motions and the satellite presence, electron current to a satellite probe is less than for zero magnetic field. When the probe is perpendicular to the magnetic field lines, its sheath will be elliptically shaped about the probe axis as shown in Figure 16. When the probe is aligned with the field, the sheath will be circular about the probe axis with the sheath thickness increased from that at zero magnetic field. The elliptical sheath cross section and the increase in sheath thickness occur because sheath formation by ion repulsion requires motions across the magnetic field lines, which is difficult to achieve. The increased amount of positive charge remaining near the probe requires that more volume must be included in the sheath in order to encompass enough negative charge to cancel a positive probe potential.

Most electrons reaching the probe at 180^o or zero field angles must cross field lines to do so. In contrast, many electrons arriving

at the probe for 90^{o} field angle can do so by traveling along field lines and the elliptical sheath configuration intercepts more than the normal number of field lines. The magnetic field presence results in a current which reaches a maximum at 90^{o} field angle and minima at 0^{o} and 180^{o} field angle. For no translational probe velocities, there may still be an end effect because it is easier for electrons to enter the end of the probe when the probe is aligned with the field lines. The plotted $M(\phi)$ curves do not conflict with the stated model.

The state of theories concerning magnetic modulations of probe current collection was reviewed by Chen in 1965. The primary difficulty in accounting for magnetic field effects is that a collisionless theory may not be adequate. Magnetic collisions within the sheath can only be ignored if the gyro-radius, R_g, is greater than the Debye length, h. The mean gyro-radius for an ionospheric electron is $mc\bar{v}/Be$ where B is the geomagnetic field strength; and h is $(kT/4\pi ne^2)^{\frac{1}{2}}$ where n is the electron number density.

$$R_g/h = \frac{mc}{Be}\left(\frac{8kT}{\pi m}\right)^{\frac{1}{2}}[4\pi ne^2/kT]^{\frac{1}{2}} \sim \frac{5.7(mn)^{\frac{1}{2}}c}{B}$$

For the conditions of the present analysis

$$10^3/cc \leq n \leq 10^5/cc \text{ and } B \sim 0.4 \text{ gauss.}$$

Since

$$m \sim 10^{-27} \text{ gm and } c = 3 \times 10^{10} \text{ cm/sec, } R_g/h \sim 1.5$$

demonstrating that the magnetic collisions within the sheath should be almost negligible. Under these circumstances,

magnetic collisions within the probe sheath are of little consequence in modifying electrostatic probe characteristics for ionospheric electron current collection. On the other hand, the altered charged particle diffusion in the presence of the geomagnetic field, as discussed previously, may be important in any case.

An alternate mechanism for explaining the $M(\phi)$ curves is anisotropy in the pitch angle distribution for the electrons of thermal energies. The magnetic moment, μ, of a charged particle in a magnetic field is $U_\perp / B$ where $U_\perp$ is the kinetic energy of the particle in a direction $\perp B$. If μ is conserved, then $v^2 \sin^2\alpha / B$ is constant, where α, the pitch angle, is the angle between the particle velocity and the magnetic field lines. Lenchek has shown that for charged particles escaping from a collision dominated region into a collisionless ionosphere, when μ is conserved, there is a critical pitch angle, α_c, which satisfies the relationship $\sin^2\alpha_c = B/B_o$. B is the magnetic field strength at a given radial distance, R, from a magnetic dipole and B_o is the magnetic field strength at the base of the collisionless region. The critial angle divides the pitch angle distribution at a given height into two regions. For $\alpha \leq \alpha_c$ there is no specific upper bound to the velocities which the charged particles might have. For $\alpha > \alpha_c$ there is a maximum permissible velocity, v_m, which charged particles can have where

$$v_m^2 = f(\sin^2\alpha,\ R/R_o,\ B/B_o).$$

The effect of taking into account coulomb collisions in the "collisionless"

region is to reduce the anisotropy by increasing the value of v_m.

The important part of the Lenchek model of topside ionospheric escape fluxes of charged particles for the present study is the prediction of a flat pitch angle distribution of particles for $\alpha \leq \alpha_c$. When $\alpha > \alpha_c$, a rapid fall-off in the pitch angle distribution is predicted. This is precisely the behavior of many of the $M(\phi)$ curves.

If one accepts the shape of the $M(\phi)$ curves as an adequate indication of the dominant mechanism in producing the shape, one can state that of the curves plotted, six out of eleven show an anisotropic pitch angle distribution of electrons to be the dominant mechanism in producing magnetic field modulations in the ionospheric electron current to cylindrical probes. The distinction in curve shapes is that for a variation of field angle from 90^o towards either 0^o or 180^o there should be a continuous decrease in electron current if slow diffusion across magnetic field lines is the dominant mechanism. Only two out of eleven displayed this behavior. In contract, the anisotropic pitch angle mechanism requires a region of almost constant current, centered around 90^o field angle. Then at some critical angle there should be a rapid fall-off in current. The extra modulations in the $M(\phi)$ curves at 1550 km altitude indicate some mechanism in addition to those operating at the other altitudes studied. In this case, there appears a particular pitch angle about which there is a depletion of electrons.

Because of the location of the probes near the bottom of the

satellite, there should be an assymmetry in the $M(\phi)$ for all field angles if the satellite presence is an important factor in the modulation of normal electron current collection. The general symmetrical nature of the $M(\phi)$ curves indicates that the satellite presence has little effect on the curve shape. In some cases there is an assymmetry in $M(\phi)$ for field angles near 90^{o}, but these assymmetries can be interpreted in terms of a net flux of electrons in one direction. The satellite presence affects such a flux because the satellite will tend to scatter the particles out of the field tube for electron collection at one field angle but not at the supplement of that field angle. The result is an assymmetric $M(\phi)$ curve. The assymmetry disappears for field angles such that $\alpha > \alpha_c$ because of the restriction on the velocities permissible to the lowest velocities. The net flux would tend to involve particles in the higher velocities of a Maxwellian distribution where collisions would be less important. In this study, assymmetries in $M(\phi)$ are of the order of 5% when they occur.

The results presented are important in explaining the effects of satellite velocity and the geomagnetic field on cylindrical probe measurements in the ionosphere. The modulations observed due to satellite velocity effects represented changes in the accelerated electron current from doubling of the current, through no effect whatsoever, to reducing the current by one-half. When the satellite velocity effects were removed, the magnetic effects, which were always present, remained. The stationary probes' accelerated electron currents

contained a 20 - 60% modulation from magnetic field effects where both diffusion effects and pitch angle distributions for the electrons are the important contributing factors. Since electrostatic probe measurements are one of the principal methods for deducing plasma charged particle densities, the results of this analysis should be useful in determining how to extract an unambiguous value of ionospheric electron density from electrostatic probe data. In addition, the results suggest a possible means of determining the presence of charged particle fluxes and anisotropies in pitch angle distribution among the ionospheric electrons. Both of these phenomena are important in the theory of transport processes in the ionized atmosphere.

APPENDIX

A SAMPLE CALCULATION FOR MODULATION SEPARATIONS

The first few steps in the separation procedure can be illustrated by numerical calculations on the data taken from Pass #268 at the 750 km level. The curves labeled #268A of Figures 6 and 7 are used. Since there is a data point at 87^{o} aspect angle, rather than 90^{o}, one can use 87^{o} as the starting point with little error. From our definitions, $V(\theta)$ is taken as zero at 87^{o} aspect angle. Therefore, the electron current to the probe is only influenced by the magnetic modulation appropriate to ϕ, where $I(87^{o},\phi_1) = M(\phi_1)$. The ϕ_1 is 37^{o} and the value of the data point is 0.405. On a magnetic modulation plot the value of $I(87^{o},37^{o})$ is taken for both $M_1(37^{o})$ and $M_1(143^{o})$.

If only magnetic effects were important, $I(\theta,\phi)$ would show a value of 0.405 at $\phi = 143^{o}$. However, $I(\theta,143^{o}) = 0.348$ which indicates that velocity effects have lowered the current by 0.057 units. θ_2 is found by looking at $I(\theta,\phi)$ plotted against aspect angle for $20^{o} < \theta < 37^{o}$ with $I(\theta,\phi) = 0.348$ units. θ_2 is 27^{o} from Figure 6 and $V_o(\theta_2) = -0.057$ units. $V_o(27^{o}) = V_o(-27^{o})$, hence, subtracting $V_o(-27^{o})$ from $I(-27^{o},\phi_3)$ gives the electron current without a velocity modulation. $I(-27^{o},\phi_3) = 0.488$ units and the subtraction of $V_o(-27^{o})$ gives 0.545 units which only contains a magnetic modulation.

ϕ_3 corresponding to $I(-27^{o},\phi_3) = 0.545$ current units is obtained by looking at $I(\theta,\phi)$ plotted against field angle to find $95^{o} < \phi < 116^{o}$ where $I(\theta,\phi) = 0.488$ units. From Figure 7 this angle is 101^{o}. 0.545 is the value of $M_1(101^{o})$ and $M_1(79^{o})$. $I(\theta,79^{o}) = 0.480$ and a value of $V_o(\theta)$ for another aspect angle can be determined as before. This process is continued until an approximate $M_1(\theta)$ curve can be drawn.

REFERENCES

Antonova, L. A., and Ivanov-Kholodnyy, "Corpuscular Hypothesis for the Ionization of the Night Ionosphere," Geomagnetism and Aeronomy (English Edition), 1, 149, (1961).

Bettinger, R. T., "An End Effect Associated with Cylindrical Langmuir Probes Moving at Satellite Velocities," Dept. of Phys. and Astron. Tech. Report 566, (1966).

Chamberlain, J. W., "Planetary Coronae and Atmospheric Evaporation," Planetary Space Science, 11, 901, (1963).

Chen, Francis F., "Electric Probes," in Plasma Diagnostic Techniques, edited by Richard H. Huddlestone and Stanley I. Leonard, pp. 113, Academic Press, New York, (1965).

Geisler, John E., and S. A. Bowhill, "An Investigation of Ionosphere-Protonosphere Coupling," Aeronomy Report No. 5, Univ. of Illinois, (1965).

Kanal, M., "Theory of Current Collection of Moving Cylindrical Probes," J. of App. Phys., 35, 1967, (1964).

Lenchek, A. M. - private communication.

Mott-Smith, H. M., and I. Langmuir, "Theory of Collectors in Gaseous Discharges," Phys. Rev., 28, 727, (1926).

Nicolet, M., and A. C. Aikin, "The Formation of the D Region of the Ionosphere," J. G. R., 65, 1469, (1959).

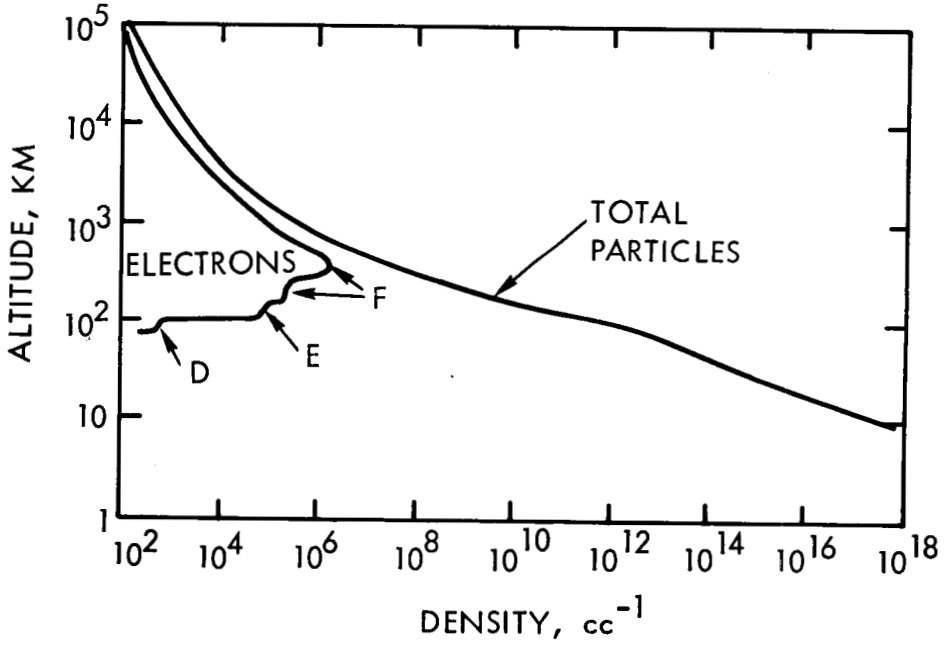
ALTITUDE, KM
10^5
10^4
10^3
10^2
10
1
ELECTRONS
F
E
D
TOTAL
PARTICLES
10^2
10^4
10^6
10^8
10^{10}
10^{12}
10^{14}
10^{16}
10^{18}
DENSITY, cc^{-1}

Figure 1

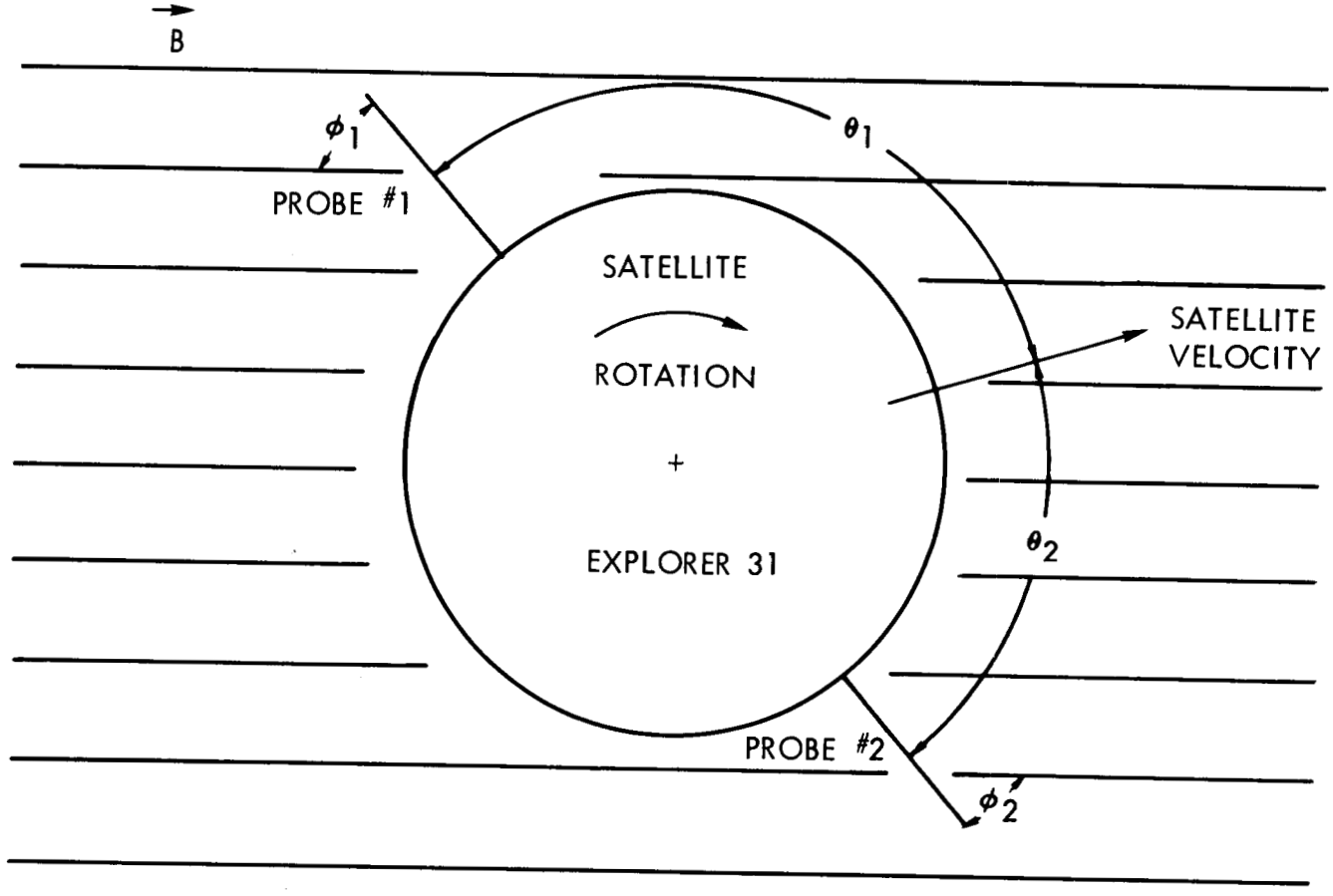
B
ϕ_1
PROBE #1
θ_1
SATELLITE
ROTATION
+
EXPLORER 31
SATELLITE
VELOCITY
θ_2
PROBE #2
ϕ_2

Figure 2

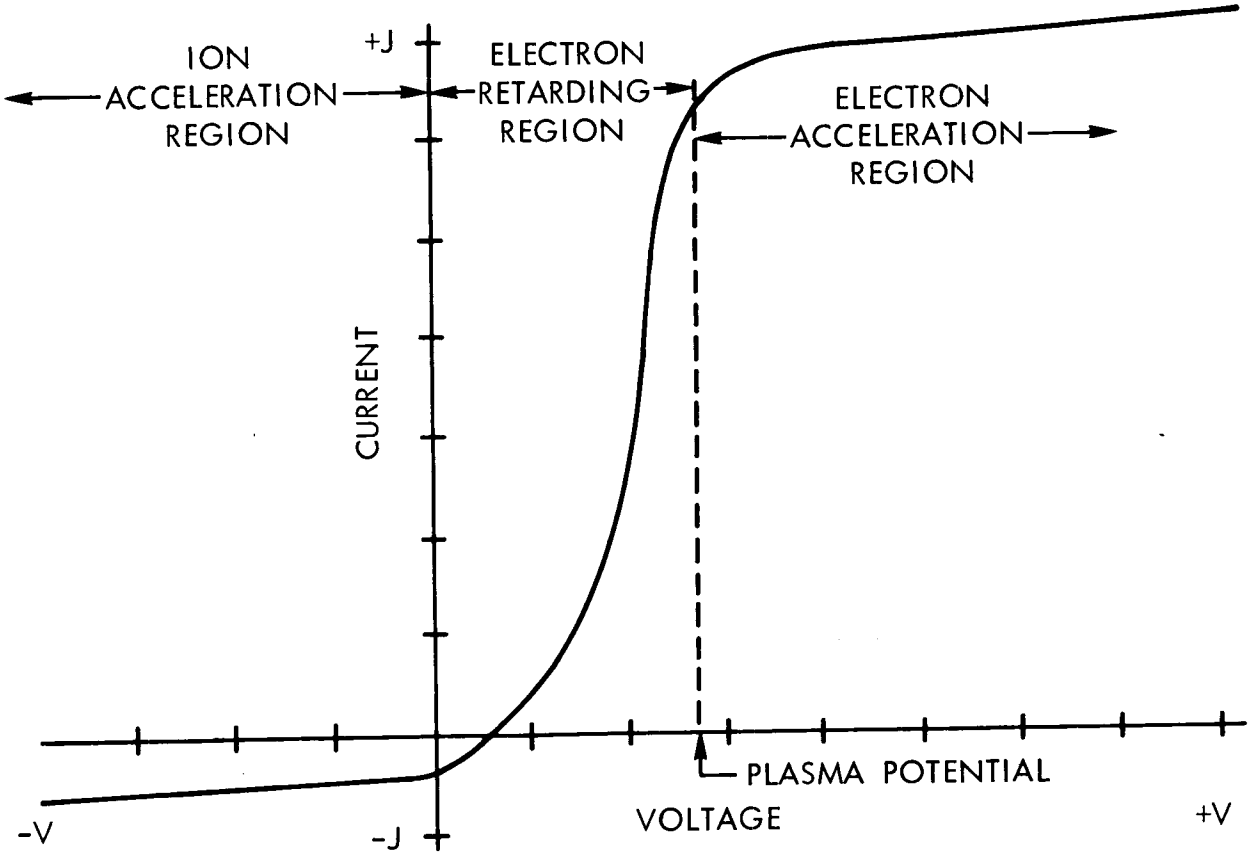
+J
ION
ACCELERATION
REGION
ELECTRON
RETARDING
REGION
ELECTRON
ACCELERATION
REGION
CURRENT
PLASMA POTENTIAL
VOLTAGE
-V
-J
+V

Figure 3

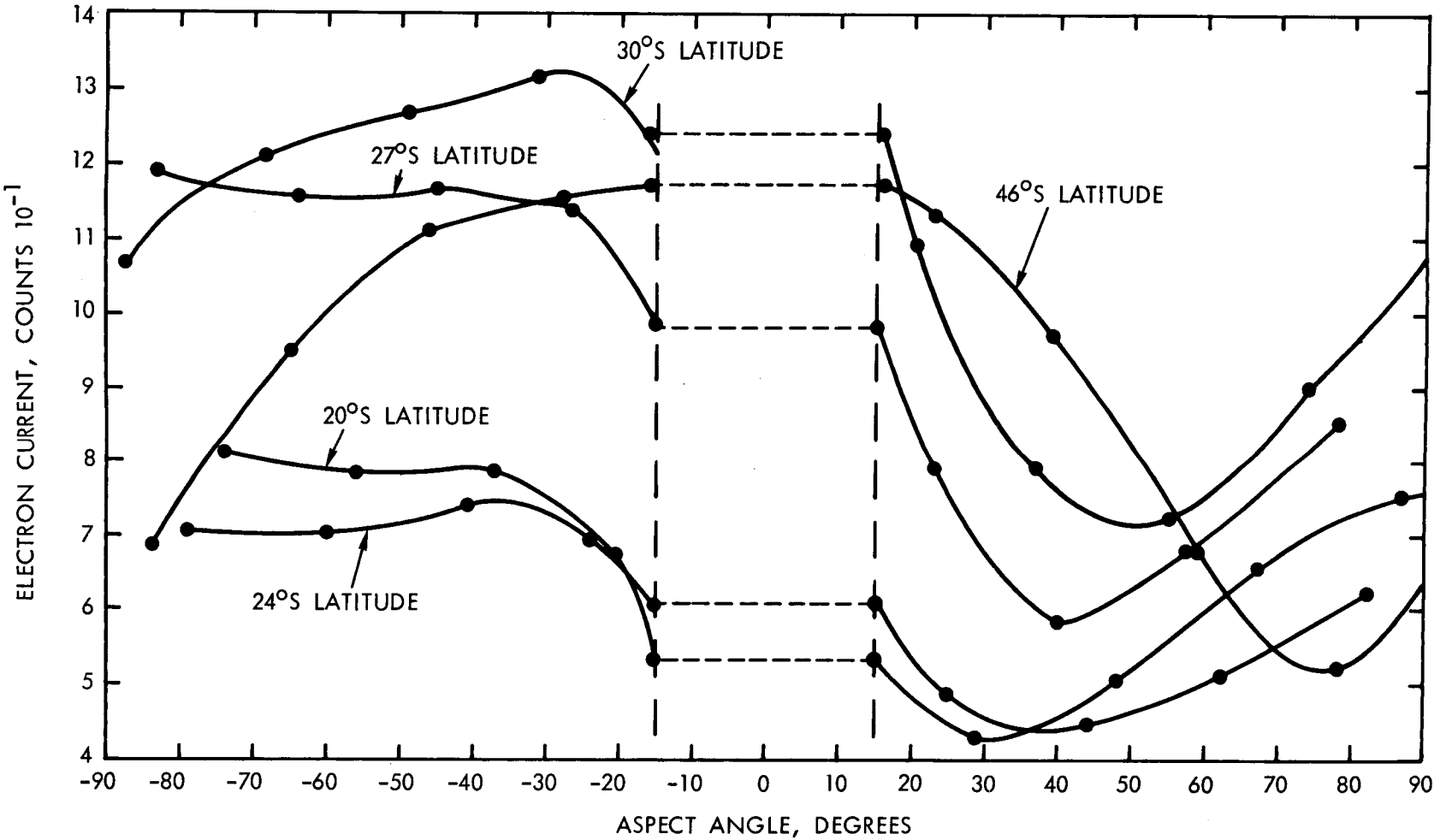
30°S LATITUDE
27°S LATITUDE
46°S LATITUDE
20°S LATITUDE
24°S LATITUDE
ELECTRON CURRENT, COUNTS 10^{-1}
ASPECT ANGLE, DEGREES
14
13
12
11
10
9
8
7
6
5
4
-90 -80 -70 -60 -50 -40 -30 -20 -10 0 10 20 30 40 50 60 70 80 90

Figure 4

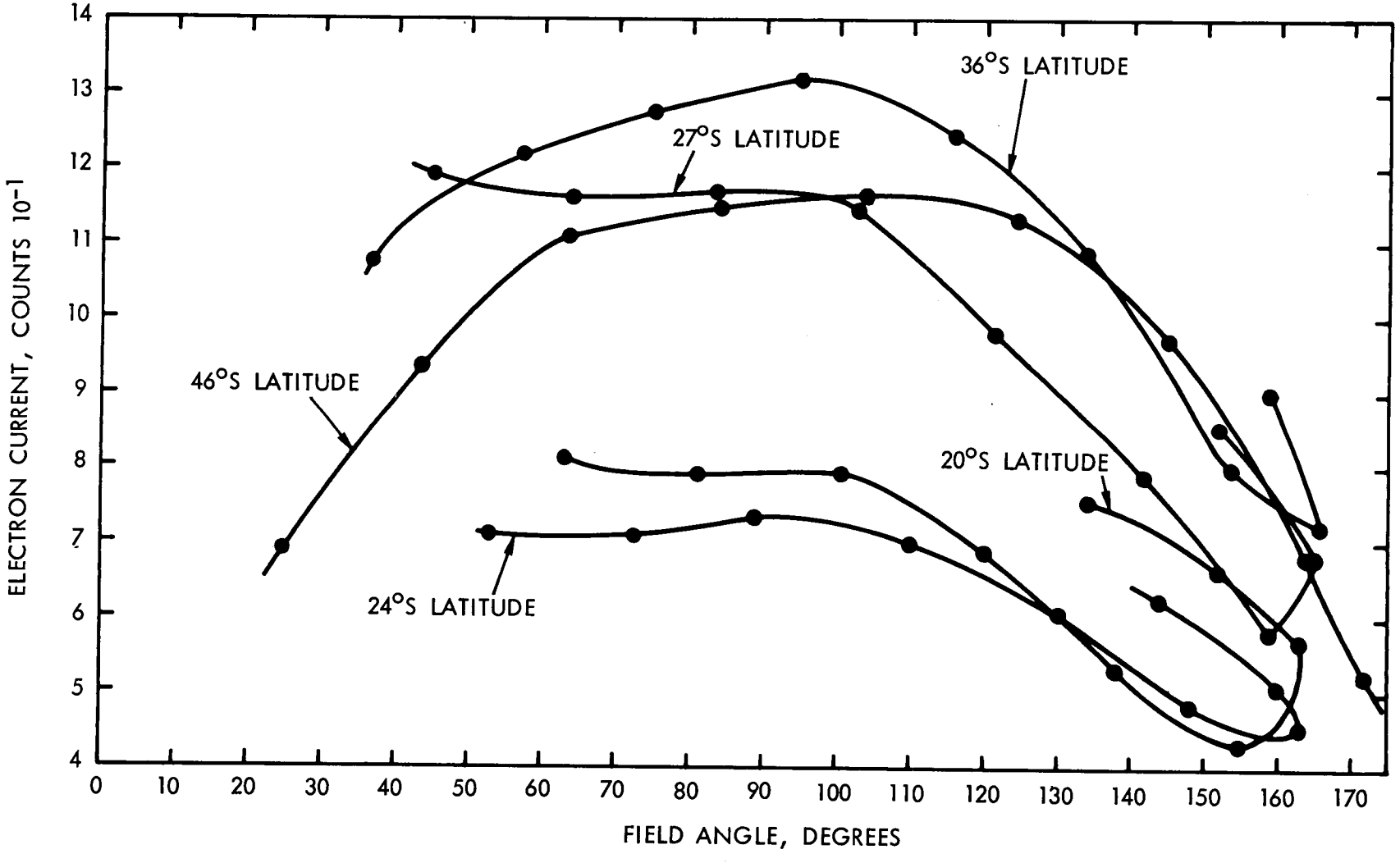
ELECTRON CURRENT, COUNTS 10^{-1}
14
13
12
11
10
9
8
7
6
5
4
0
10
20
30
40
50
60
70
80
90
100
110
120
130
140
150
160
170
FIELD ANGLE, DEGREES
36°S LATITUDE
27°S LATITUDE
46°S LATITUDE
20°S LATITUDE
24°S LATITUDE

Figure 5

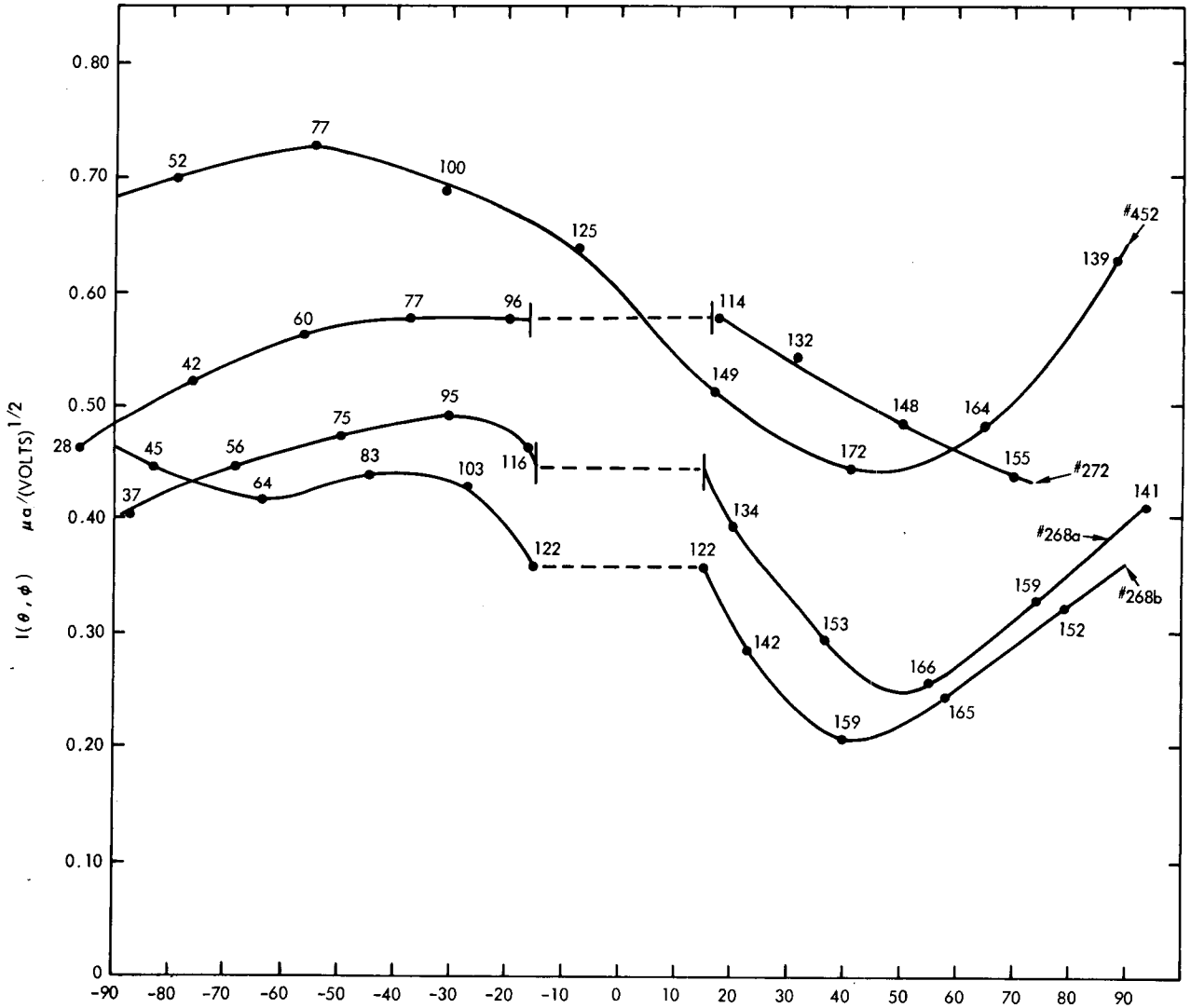
0.80
0.70
0.60
0.50
0.40
0.30
0.20
0.10
0
I(θ, φ) μa/(VOLTS)^1/2
-90 -80 -70 -60 -50 -40 -30 -20 -10 0 10 20 30 40 50 60 70 80 90
ASPECT ANGLE
#452
#272
#268a
#268b

Figure 6

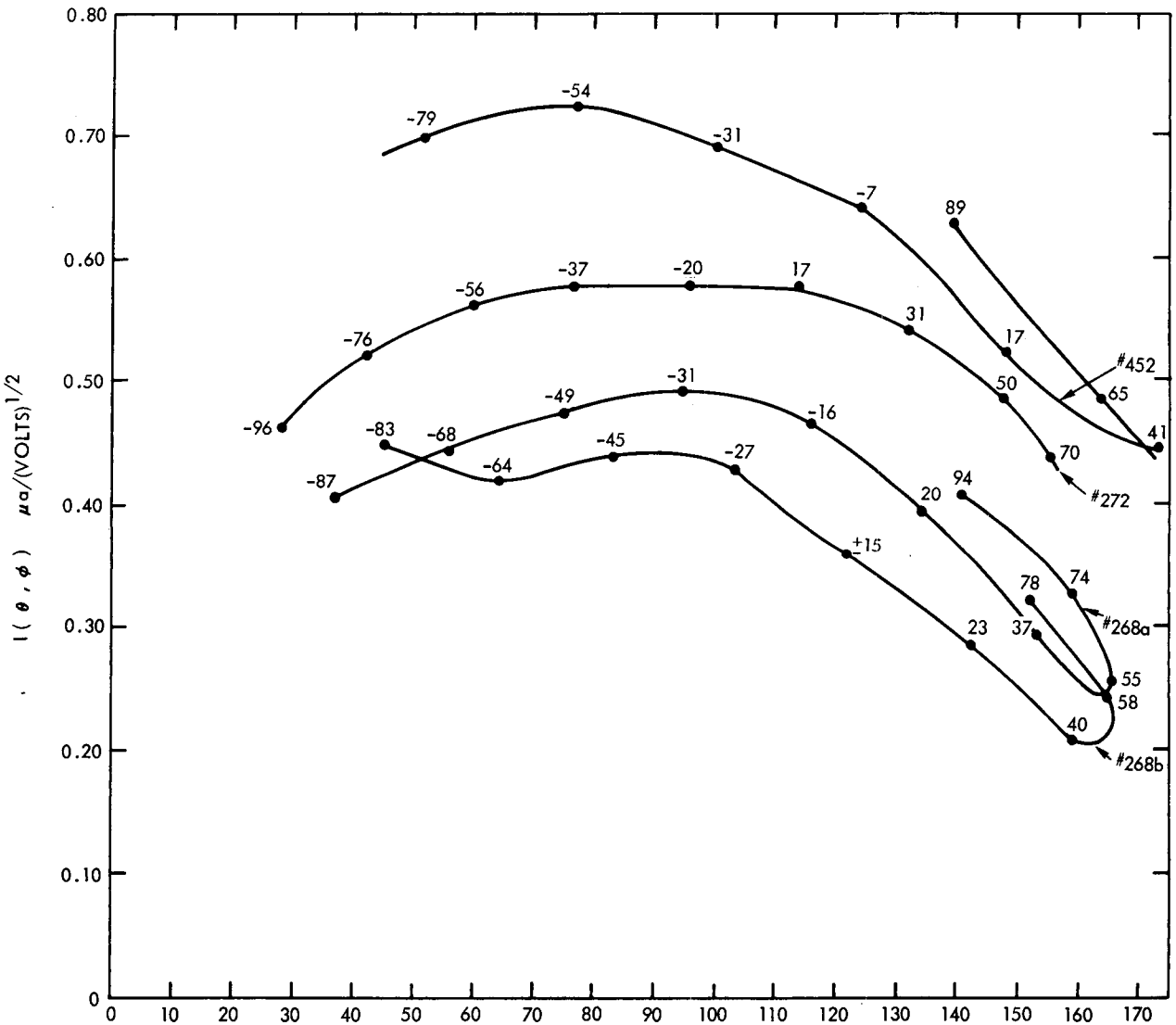
0.80
0.70
0.60
0.50
0.40
0.30
0.20
0.10
0
0 10 20 30 40 50 60 70 80 90 100 110 120 130 140 150 160 170
I(θ , φ) μa/(VOLTS)^1/2
FIELD ANGLE
-79
-54
-31
-7
89
17
#452
65
41
-96
-76
-56
-37
-20
17
31
50
70
#272
-87
-83
-68
-64
-49
-45
-31
-27
-16
±15
20
94
74
78
#268a
37
23
55
58
40
#268b

Figure 7

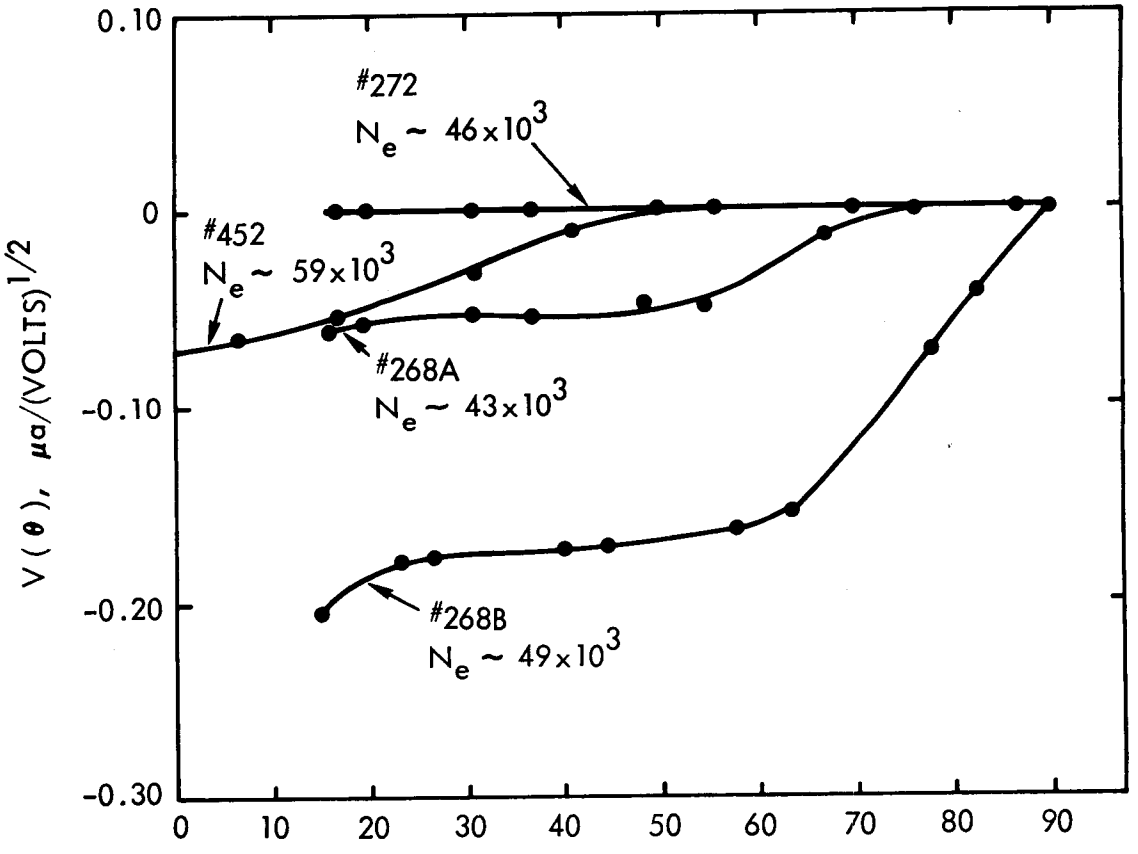
0.10
0
-0.10
-0.20
-0.30
0
10
20
30
40
50
60
70
80
90
#272
$N_e \sim 46 \times 10^3$
#452
$N_e \sim 59 \times 10^3$
#268A
$N_e \sim 43 \times 10^3$
#268B
$N_e \sim 49 \times 10^3$
V(θ), μa/(VOLTS)$^{1/2}$
ASPECT ANGLE, DEGREES

Figure 8

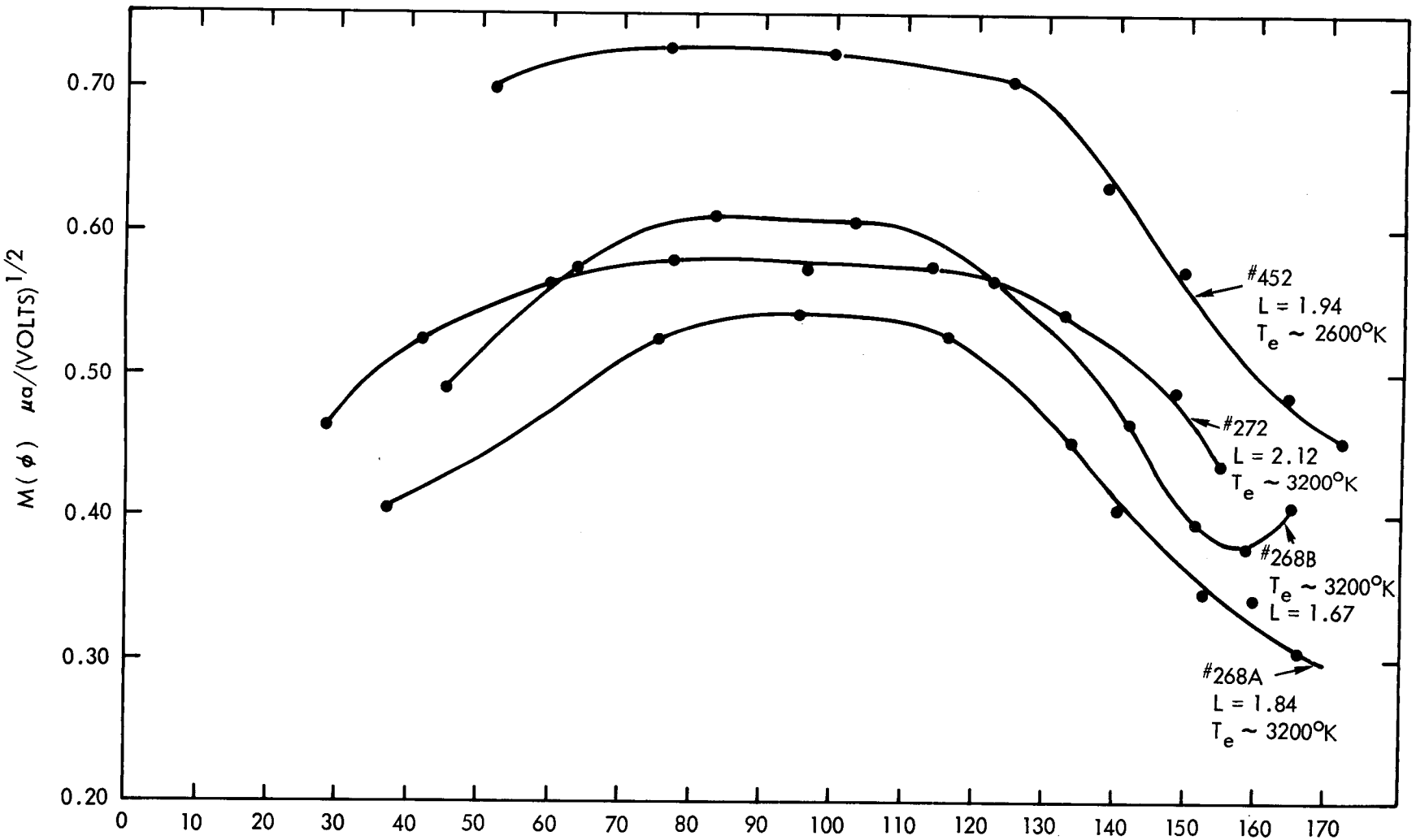
0.70
0.60
0.50
0.40
0.30
0.20
0
10
20
30
40
50
60
70
80
90
100
110
120
130
140
150
160
170
M(φ) μa/(VOLTS)^1/2
FIELD ANGLE, DEGREES
#452
L = 1.94
Te ~ 2600°K
#272
L = 2.12
Te ~ 3200°K
#268B
Te ~ 3200°K
L = 1.67
#268A
L = 1.84
Te ~ 3200°K

Figure 9

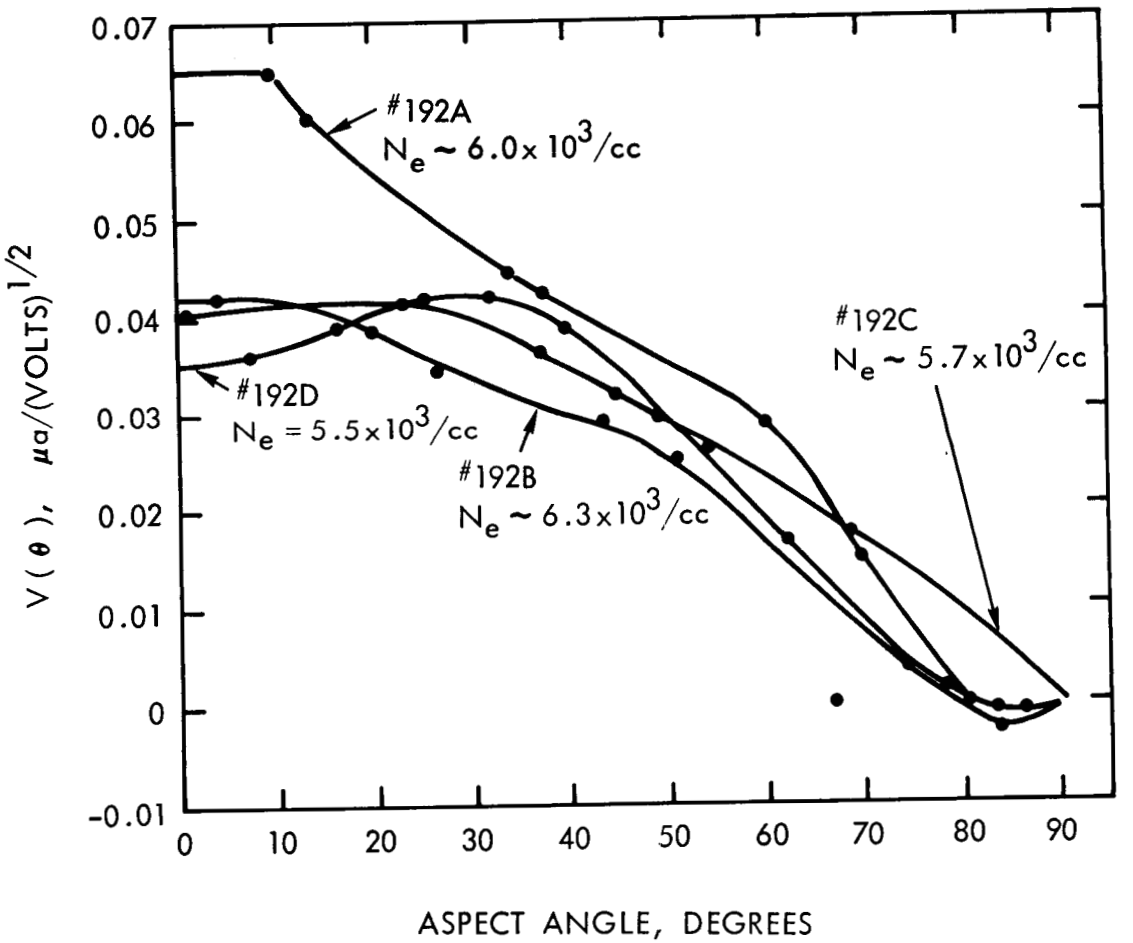
0.07
0.06
0.05
0.04
0.03
0.02
0.01
0
-0.01
0
10
20
30
40
50
60
70
80
90
#192A
$N_e \sim 6.0 \times 10^3$/cc
#192C
$N_e \sim 5.7 \times 10^3$/cc
#192D
$N_e = 5.5 \times 10^3$/cc
#192B
$N_e \sim 6.3 \times 10^3$/cc
$V(\theta)$, $\mu a/(VOLTS)^{1/2}$
ASPECT ANGLE, DEGREES

Figure 10

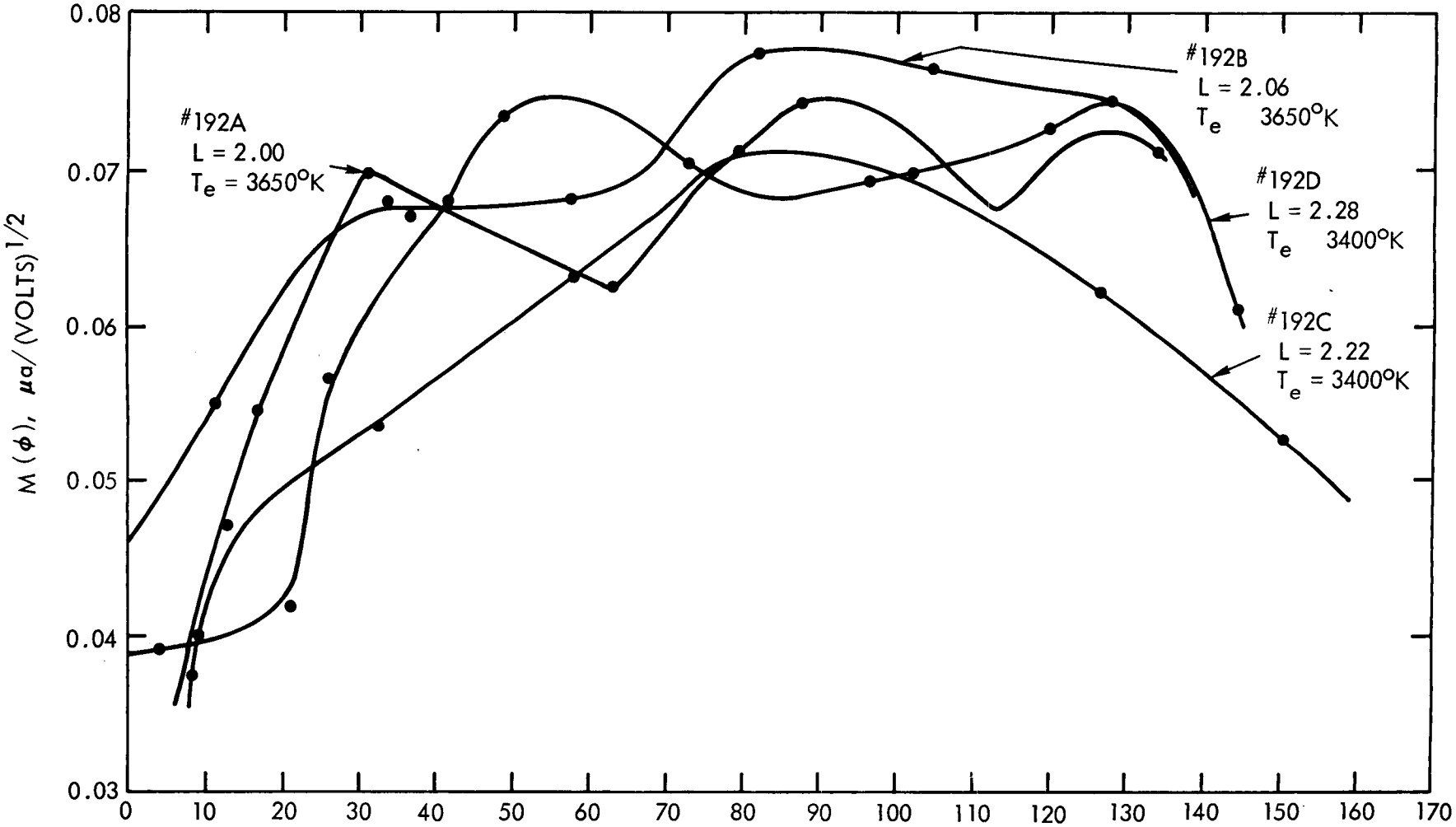
0.08
0.07
0.06
0.05
0.04
0.03
M (φ), μa/(VOLTS)^1/2
#192A
L = 2.00
Te = 3650°K
#192B
L = 2.06
Te 3650°K
#192D
L = 2.28
Te 3400°K
#192C
L = 2.22
Te = 3400°K
0
10
20
30
40
50
60
70
80
90
100
110
120
130
140
150
160
170
FIELD ANGLE, DEGREES

Figure 11

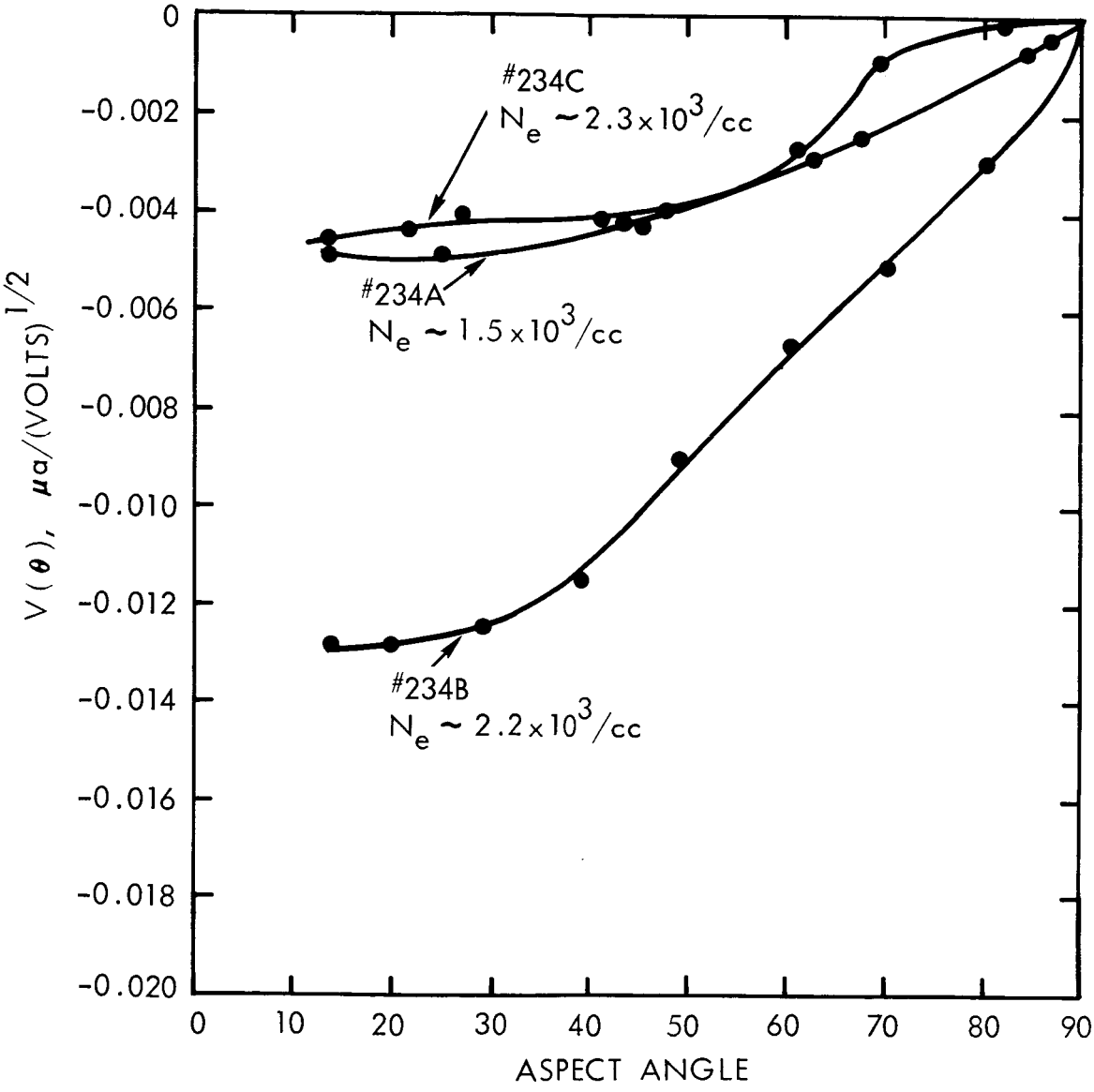
0
-0.002
-0.004
-0.006
-0.008
-0.010
-0.012
-0.014
-0.016
-0.018
-0.020
V(θ), μa/(VOLTS)^1/2
#234C
Ne ~2.3x10^3/cc
#234A
Ne ~1.5x10^3/cc
#234B
Ne ~2.2x10^3/cc
0
10
20
30
40
50
60
70
80
90
ASPECT ANGLE

Figure 12

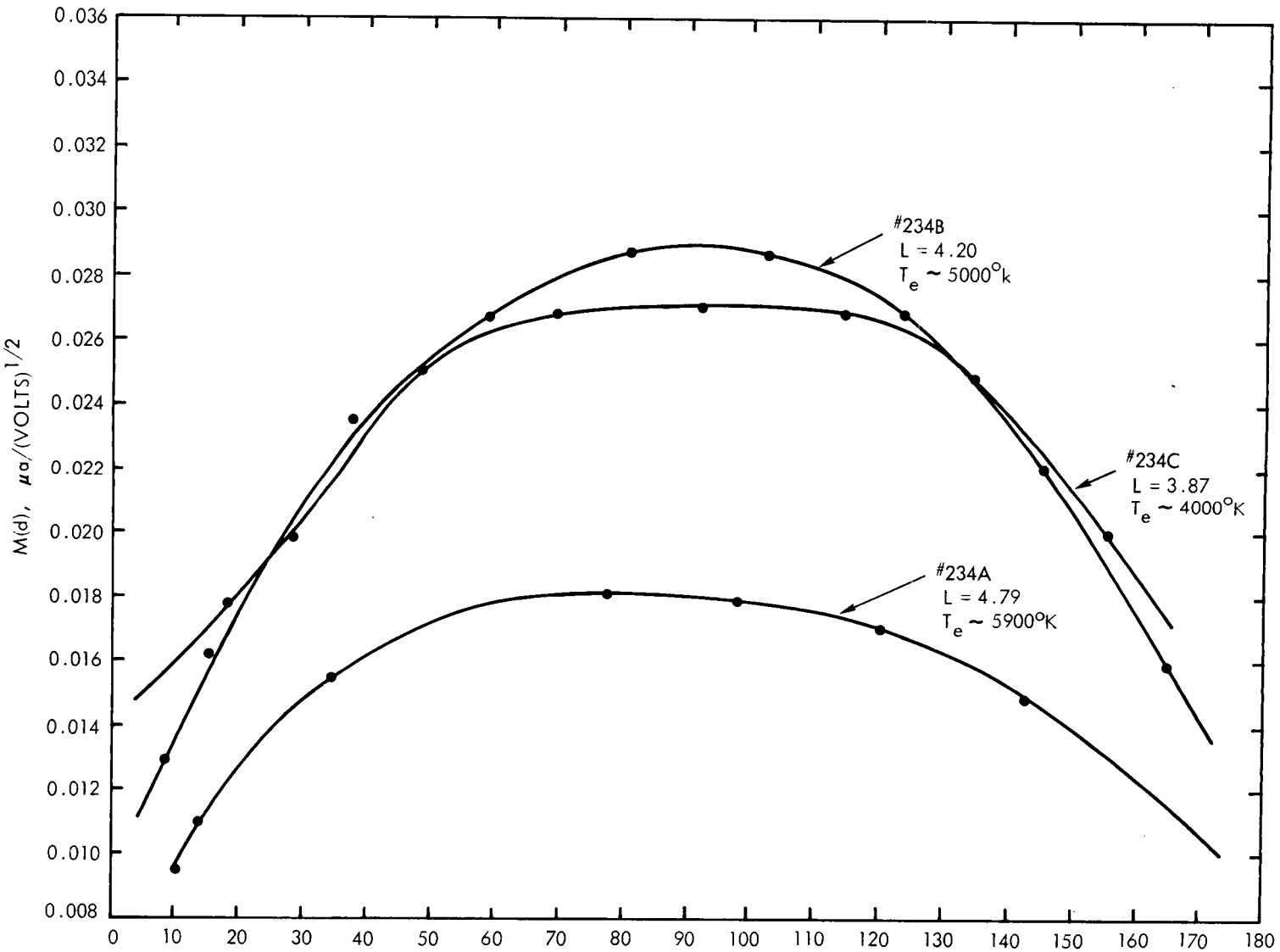
0.036
0.034
0.032
0.030
0.028
0.026
0.024
0.022
0.020
0.018
0.016
0.014
0.012
0.010
0.008
M(d), μa/(VOLTS)^1/2
0
10
20
30
40
50
60
70
80
90
100
110
120
130
140
150
160
170
180
FIELD ANGLE
#234B
L = 4.20
Te ~ 5000°k
#234C
L = 3.87
Te ~ 4000°K
#234A
L = 4.79
Te ~ 5900°K
Figure 13

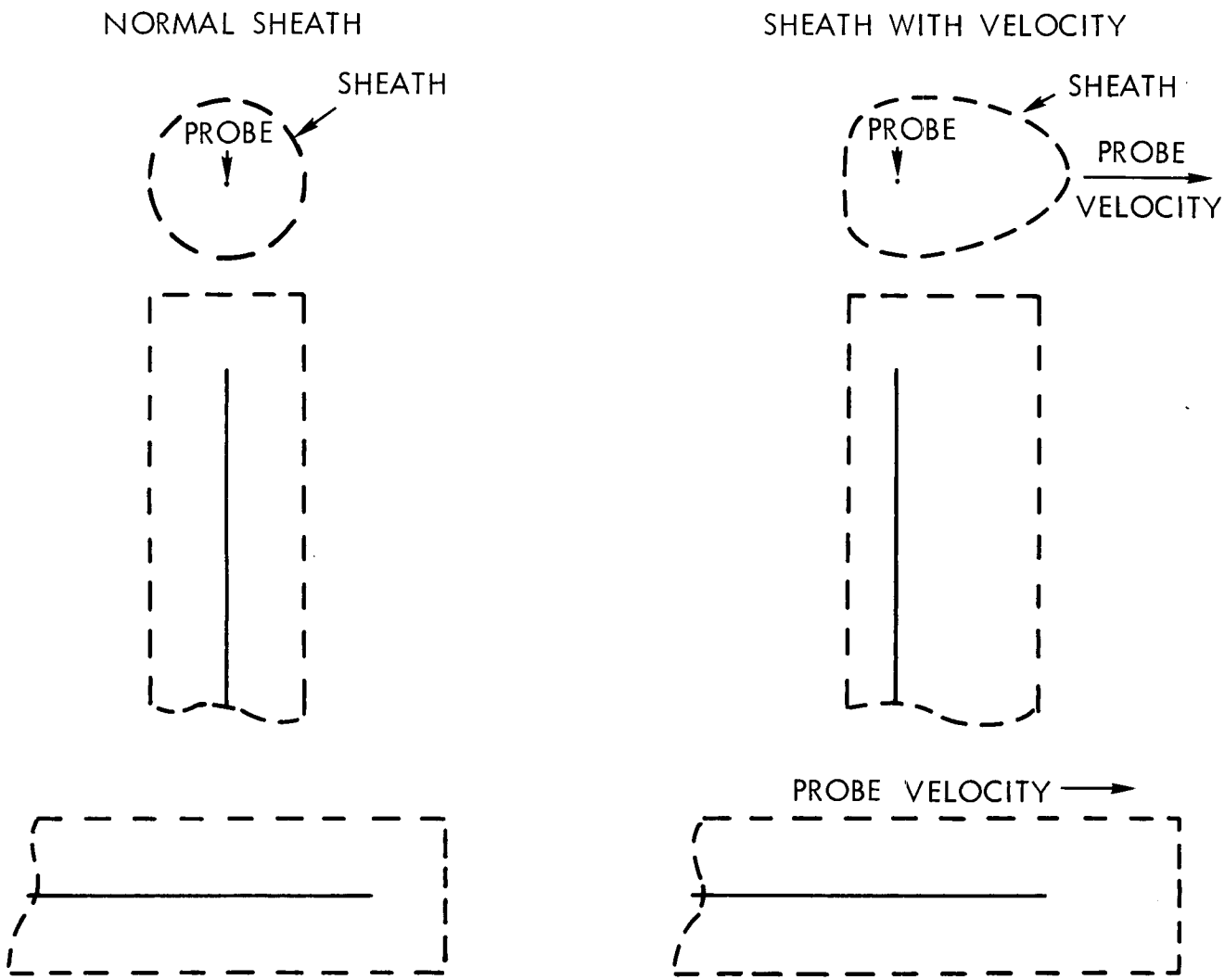
NORMAL SHEATH
SHEATH
PROBE
SHEATH WITH VELOCITY
SHEATH
PROBE
PROBE
VELOCITY
PROBE VELOCITY

Figure 14

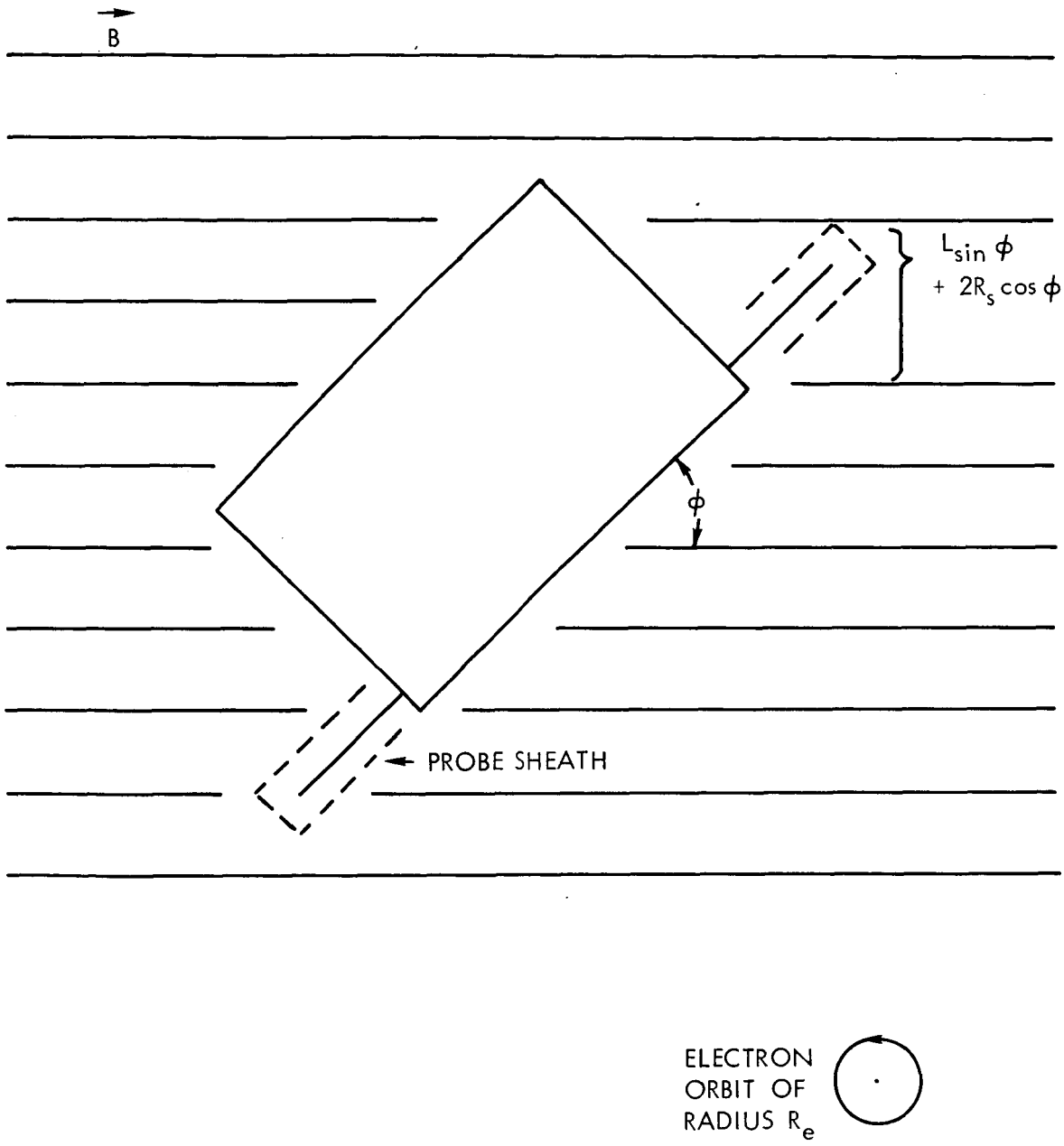
B
$L \sin \phi$
$+ 2R_s \cos \phi$
ϕ
PROBE SHEATH
ELECTRON
ORBIT OF
RADIUS R_e

Figure 15

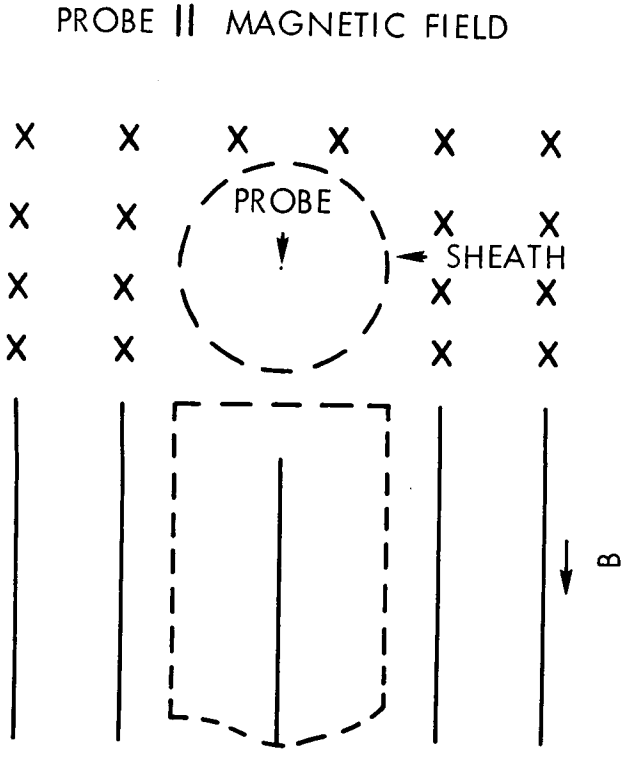
PROBE ∥ MAGNETIC FIELD
PROBE
SHEATH
B

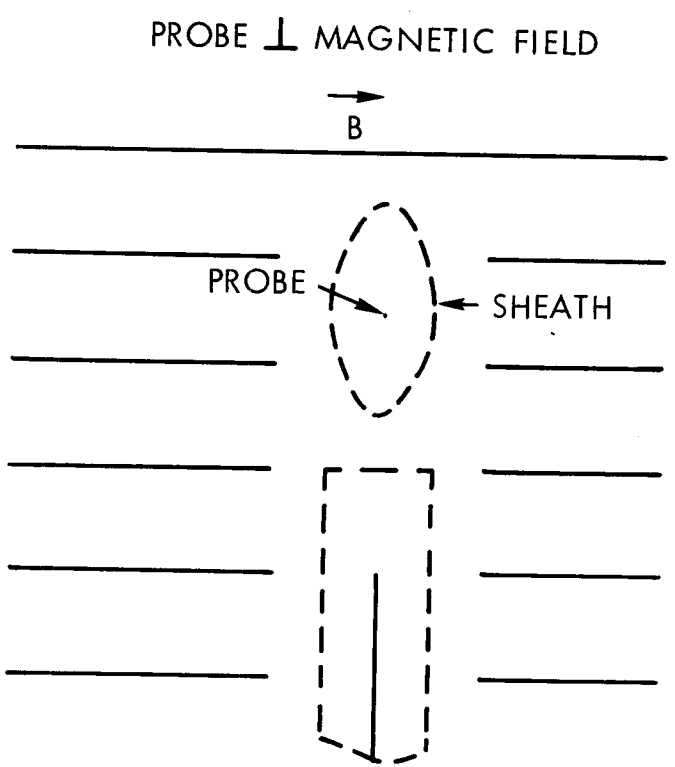
PROBE ⊥ MAGNETIC FIELD
B
PROBE
SHEATH

Figure 16